Atomistic and electronic structure of antisite defects in yttrium aluminum garnet: Density-functional study

Ana Belén Muñoz-García
Departamento de Química, C-XIV, Universidad Autónoma de Madrid, 28049 Madrid, Spain

Emilio Artacho
Department of Earth Sciences, University of Cambridge, Downing Street, Cambridge CB2 3EQ, United Kingdom

Luis Seijo
Departamento de Química, C-XIV, Universidad Autónoma de Madrid, 28049 Madrid, Spain
and Instituto Universitario de Ciencia de Materiales Nicolás Cabrera, Universidad Autónoma de Madrid, 28049 Madrid, Spain
(Received 29 April 2009; revised manuscript received 19 June 2009; published 13 July 2009)

First-principles density-functional theory calculations have been performed on the atomistic structure, electronic structure, and distribution of antisite defects (AD) in yttrium aluminum garnet (YAG) $Y_3Al_5O_{12}$. The formations of one and two antisite defects per unit cell are endothermic and the formation energy per defect is lower in 2AD than in 1AD. In the most stable 1AD structure, Y and Al are as close as possible and two oxygen atoms become unbound to Al rising the energy of their (highest) valence levels and introducing a defect level in the gap 0.25 eV above the top of the perfect YAG valence band. The binding energy between the individual substitutional defects Y_{Al} and Al_Y to form 1AD is 0.74 eV. The most stable 2AD structure is made of two single ADs linked together with one AlO_6 moiety and it has basically the same electronic structure as the most stable 1AD; it is the only 2AD structure that preserves the inversion center with respect to the unit-cell center. In this case, the binding energy between two single ADs is 0.22 eV.

DOI: 10.1103/PhysRevB.80.014105 PACS number(s): 71.55.−i, 71.15.Dx, 61.72.Bb

I. INTRODUCTION

Natural and synthetic garnets are important materials from the point of view of their usefulness; in particular, synthetic yttrium aluminum garnet (YAG), ($Y_3Al_5O_{12}$), either pure or doped with active impurities such as Nd^{3+} or Ce^{3+}, is used in a wide variety of applications, such as thermal coating, optical lenses, solid-state lasers, and solid-state-lighting devices.[1–3] It is well known that native defects appear in YAG during crystal growth depending on the temperature and crystallization procedure. Extended x-ray-absorption fine structure, x-ray-absorption near-edge spectroscopy and positron annihilation spectroscopy studies have established that among the intrinsic defects, antisite defects (AD) are dominant.[4,5] They are known to act as shallow electron traps and they affect the structure, the luminescence, and other properties of pure[6] and doped YAG.[7,8]

Antisite defects appear in YAG when yttrium and aluminum atoms exchange positions. Perfect garnets are usually described in terms of a 160 atom body-centered-cubic unit cell (80 atom primitive cell), which contains 8 f.u. of $A_3B'_2B''_3O_{12}$, where A, B′, and B″ are cations in different symmetry sites. In YAG, A≡Y is eightfold coordinated in a distorted cubic D_2 local site; this site is traditionally labeled as the dodecahedral site because the distorted cube produces a polyhedron with 12 triangular faces and we will use this term along the paper. B′≡Al is in an octahedral environment and B″≡Al in a tetrahedral environment. Idealized cubic YAG belongs to the $Ia\bar{3}d$ (230) space group with Y in 24(c) sites, Al_{oct} in 16(a) sites, Al_{tet} in 24(d) sites, and the remaining 96 oxygen atoms in (h) sites, which depend on three x, y, and z internal parameters[9] (Fig. 1). However, real YAG belongs to the trigonal $R\bar{3}$ (148) space group as a consequence of the presence of antisite defects.[4] In these defects, B′ cations (Al_{oct}) exchange positions with A cations (Y). Whereas in the higher ideal $Ia\bar{3}d$ symmetry the four cube diagonals are $\bar{3}$ symmetry axis, only the [111] axis maintains this character in the lower real $R\bar{3}$ symmetry. This axis contains some of the Al_{oct} sites in the idealized crystal. Apart from partial experimental information on the local order around the yttrium atoms,[10] little is known on the structure of the antisite defects and on their distribution.

Surprisingly, antisite defects of YAG have been the subject of very few theoretical studies. Pair-potential atomistic simulations have been performed in the framework of an empirically parametrized shell model in order to describe the

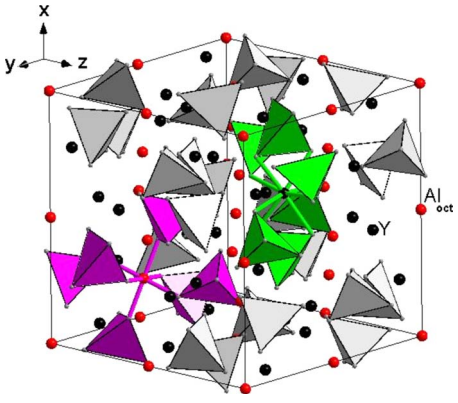

FIG. 1. (Color online) Unit cell of YAG. The yttrium ions, the aluminum ions in quasioctahedral sixfold coordinations, and the AlO_4 quasitetrahedral moieties are indicated.

energetics of formation of these and other defects such as interstitials and vacancies.[11,12] These calculations concluded that antisite defects have a lower energetic demand than other kinds of intrinsic defects and that the exchange between Y and Al_{oct} is energetically preferred over the exchange between Y and Al_{tet}, in agreement with the experimental observations. Regarding first-principles studies, periodic-boundary-conditions calculations of YAG and other garnets are available,[13–18] and embedded-cluster calculations on the structure and the absorption and luminescence of Ce^{3+} substitutional defects in YAG exist,[19] but we are not aware of first-principles studies on antisite defects in YAG.

Thus, the study from a first-principles point of view of the structure and energetics of antisite defects of YAG, their distribution in the host, and their electronic structure, is the primary goal of this paper. In order to do it, we carried out and analyzed first-principles periodic-boundary-conditions density-functional theory (DFT) calculations[20,21] in YAG with one and two antisite defects per cubic unit cell. The details of the calculations are described in Sec. II, the results for one and two antisite defects per unit cell are shown and discussed in Sec. III, and the conclusions are presented in Sec. IV.

II. DETAILS OF THE CALCULATIONS

The first-principles calculations in this paper have been performed with the periodic-boundary-conditions self-consistent SIESTA method,[22,23] using DFT (Refs. 20 and 21) within the generalized gradient approximation (GGA) as formulated by Perdew, Burke, and Ernzerhof (PBE).[24,25] Norm-conserving pseudopotentials[26] in the Kleinman-Bylander form[27] have been generated for the following atoms and reference configurations: $Y(5s^24p^64d^1)$, $Al(3s^23p^1)$, and $O(2s^22p^4)$, with nonlinear partial-core corrections[28] and semicore states to account for large core-valence overlap in the case of Y. Atomic basis sets of a double-ζ plus polarization quality have been optimized for the three species by the fictitious enthalpy method of Anglada *et al.*[29] in an idealized cubic $YAlO_3$ perovskite with the following sizes: $Y(5s5s'4p4p'5p4d4d')$, $Al(3s3s'3p3p'3d)$, and $O(2s2s'2p2p'3d)$. These pseudopotentials and basis sets have been obtained and used previously in calculations of perfect YAG, yttrium aluminum perovskite $YAlO_3$, Al_2O_3, and Y_2O_3 with satisfactory results.[18] The charge density is projected on a uniform grid in real space, with an equivalent plane-wave cutoff of 380 Ry, in order to calculate the exchange-correlation and Hartree matrix elements. Total energy calculations have been converged with respect to *k*-space integration; a *k* grid cutoff of 15.0 bohr was used.

All geometry optimizations have been performed without imposing any symmetry restrictions in the position of all atoms in the unit cell, using a conjugate gradient method, with a force tolerance of 0.04 eV/Å. Starting geometries were generated from the computed atomistic structure of perfect YAG (Ref. 18) [$a=12.114$ Å, $x(O)=-0.036$, $y(O)=0.0519$, and $z(O)=0.1491$, in good agreement with experiment[9]] upon exchange of Y and Al atoms to generate the antisite defects. Firstly, we optimized the structures of the single substitutional defects Y_{Al} and Al_Y, in order to obtain the structures and energies of the individual defects. The 160 atoms unit cell is large enough to consider negligible the interaction between the individual substitutional defects. We found that $Y_{Al(oct)}$ is 1.05 eV/defect more stable than $Y_{Al(tet)}$ (2.38 eV/defect more stable before relaxation); in consequence, all the antisite defects studied involve $Y_{Al(oct)}$ and Al_Y. Then, we computed the structures and energies of all possible cases of one Y_{Al}-Al_Y antisite defect per unit cell, 1AD:YAG. Finally, we computed a selection of all possible cases of two antisite defects per unit cell, 2AD:YAG, made after the conclusion of the 1AD:YAG study. We have explored the change in the volume of the unit cell produced by the antisite defects by allowing the cell to breath after every optimization of a defect. We obtained average volume increments of +0.043% in 1AD:YAG and +0.11% in 2AD:YAG. Volume effects have thus been neglected in this study, so that all the coordinates and energies in the paper correspond to $a=12.114$ Å.

III. RESULTS AND DISCUSSION

A. One antisite defect per unit cell, 1AD:YAG

1. Structure

The local dodecahedral (distorted cube) and octahedral environments of the single substitutional defects Al_Y and Y_{Al} are shown in Fig. 2. For a reference, the calculated relaxed structures of such single defects are reflected in Table I. As we will see below, the antisite defect where Al_Y and Y_{Al} are as close as possible will take an important role and, accordingly, we will label the antisite-related oxygen atoms as d1–d6 if the oxygens belong to the original YO_8 distorted cube (dodecahedron) only, o1–o4 if they belong to the original AlO_6 octahedron only, and b1 and b2 if they are bridge atoms common to the original linked dodecahedron and octahedron.

Four different Y_{Al}-Al_Y single antisite defects can be created with a defect concentration of 1AD per cell. They are shown in Fig. 3 and they can be classified according to the distance between Al_{oct} and Y in perfect YAG: 3.386, 5.460, 6.939, and 8.155 Å. Their formation energies per antisite defect, E_f (1AD), calculated as the difference between the total energies per unit cell of 1AD:YAG and perfect YAG after optimization of the atomic positions of all atoms in both cases, $E(1AD)$-$E(YAG)$, are shown in Table II. The data at infinite distance, $E_{f,\infty}(1AD)$, have been calculated out of the energies of the single substitutional defects Y_{Al} and Al_Y: $E(Al_Y:YAG)+E(Y_{Al}:YAG)-2E(YAG)$. We can observe that the most stable single AD corresponds to the shortest distance between Al and Y, which means an effective attraction between the single substitutional defects Y_{Al} and Al_Y. Binding energies within the substitutional defect with respect to the isolated defects situation, $E_b(1AD)$, are reflected in Table II, showing an attraction energy of 0.74 eV for the most stable single AD.

This is what one expects of the electrostatic interaction between these defects because (a) they are both uncharged and (b) the individual substitutions do not change basically

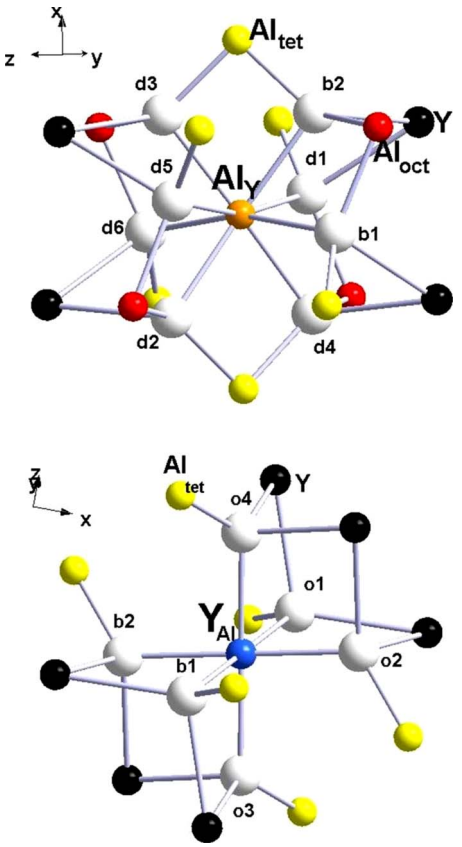

FIG. 2. (Color online) Single substitutional defects. Top: Al atom in Y site [Al_Y orange (medium-light gray)]. Bottom: Y atom in Al_{oct} site [Y_{Al} blue (medium-dark gray)]. First coordination shell (white oxygen atoms) and second coordination shell [black Y atoms, yellow (light gray) Al_{tet} atoms, and red (dark gray) Al_{oct} atoms] are shown. Oxygens labeled d1–d6 correspond to the original dodecahedral site and o1–o4 to the original octahedral site. Oxygens b1 and b2 will be bridge atoms between Al_Y and Y_{Al} in the most stable antisite defect (see below).

the symmetry and the orientations of the multipoles of the two sites. So, the *static* electrostatic interactions between them (meaning the interactions between the Y_{Al} and Al_Y defects without any deformations induced by their mutual interaction) should basically be the same as the interaction between Y and Al in perfect YAG. Then, the attractive interaction between the induced multipoles would be dominant. In other words, the elastic deformations around Y_{Al} and Al_Y due to their mutual interaction in Y_{Al}-Al_Y antisite defects are such that they attract each other. Although we like to think in electrostatic terms because all observations fit the paradigm very naturally, strain-mediated interactions between the substitutional defects could also be responsible for their attraction. This is clearly the case at very short distances since coordination rearrangements of both defects are benefiting from each other's presence (see below).

According to these first-principles calculations, the formation of a single antisite defect is a very endothermic process (3.72–4.32 eV/defect and 360–415 kJ/mol). The available pair-potential simulations led to a significantly less endothermic antisite-defect formation energy (0.9 eV/defect and 87 kJ/mol).[11] Although the first-principles value could be overestimated, it seems to indicate that the concentration of these entropic established defects is determined at high temperatures (close to the temperature of crystal growth) since they get kinetically trapped at lower temperatures by large energy barriers. Overestimation of the antisite-defect formation energy seems to be due to an overestimation of the formation energies of the two Y_{Al} and Al_Y single substitutional defects. When these are formed, the initial AlO_6 and YO_8 moieties contain more covalent bonding than the final moieties YO_6 and AlO_8 because AlO_6 is more covalent than YO_8, YO_6, and AlO_8, and the PBE functional does not seem to be sufficiently accurate to describe the energetics of this bond rearrangement. Although basis set and pseudopotentials certainly contribute to the errors in these numbers, the con-

TABLE I. Al-O, Y-O, and Al-Y distances, in Å, in perfect YAG, single substitutional defects Al_Y and Y_{Al}, and most stable single antisite defect. Atomic labels used in Fig. 4 are indicated.

	Dodecahedral site		
	YAG	Al_Y :YAG	1AD:YAG
Oxygen	d(Y-O)	d(Al_Y-O)	d(Al_Y-O)
d1	2.446	2.384	3.216
b1	2.446	2.383	2.889
d2	2.333	2.150	2.314
d3	2.333	2.150	2.189
b2	2.333	2.150	2.064
d4	2.333	2.147	2.058
d5	2.446	2.374	1.964
d6	2.446	2.375	1.954
	d(Y-Al_{tet1})	d(Al_Y-Al_{tet1})	d(Al_Y-Al_{tet1})
	3.028	2.963	3.000
	d(Al_{tet1}-O)	d(Al_{tet1}-O)	d(Al_{tet1}-O)
	1.79×4	1.80–1.81	1.80–1.83
	Octahedral site		
	YAG	Y_{Al}:YAG	1AD:YAG
	d(Al_{oct}-O)	d(Y-O)	d(Y_{Al}-O)
o1	1.947	2.176	2.233
o2	1.947	2.176	2.226
o3	1.947	2.176	2.223
b2	1.947	2.176	2.211
o4	1.947	2.176	2.186
b1	1.947	2.176	2.128
d3[a]	4.313	4.328	4.204
d1[a]	3.784	3.778	3.783
	d(Al_{oct}-Al_{tet2})	d(Y_{Al}-Al_{tet2})	d(Y_{Al}-Al_{tet2})
	3.385	3.458	3.442
	d(Al_{tet2}-O)	d(Al_{tet2}-O)	d(Al_{tet2}-O)
	1.79×4	1.78–1.80	1.75–1.78
	d(Y-Al_{oct})		d(Y_{Al}-Al_Y)
	3.384		3.655

[a]This oxygen does not belong to the first, sixfold coordination shell of Al_{oct} in YAG.

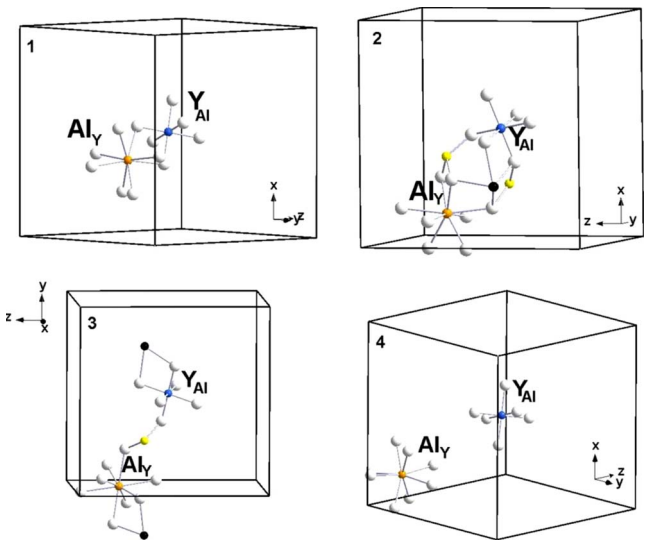

FIG. 3. (Color online) The four possible 1AD:YAG, ordered according to the Y-Al distance before relaxation: (1) 3.39 Å, (2) 5.46 Å, (3) 6.94 Å, and (4) 8.16 Å. First coordination shell (white oxygen atoms) and, where appropriate, black Y atoms and yellow (light gray) Al_{tet} shared atoms of the second coordination shell shown.

vergence tests performed on these point to the exchange-correlation approximations as the main cause of the deviation. Hybrid functionals are expected to perform better for this purpose. However, after the single substitutional defects are formed, their mutual attraction does not involve important bond changes and we should expect the PBE functional to perform well and to accurately predict the relative energies of different ADs and the binding energies between Y_{Al} and Al_Y. The same will be true for the interaction between two ADs.

Relaxation energies, E_r(1AD), are also shown in Table II. They are defined as the energies of each relaxed structure, E(1AD), minus the energy of the corresponding stressed structures after Y and Al exchange their positions, E_0(1AD). They are within the −6.18 to −5.56 eV/defect range and follow the same pattern as formation energies do. Thus, the fact that the more favorable the relaxation energy is, the more stable the AD structure is, suggests an important role of the flexibility of the local environments around YAG positions.

Let us comment on the structure of the most stable single antisite defect, which is shown in Fig. 4 and Table I. Al_Y shows a strong preference for a sixfold coordination, attracting six of the oxygens to shorter distances (1.95–2.31 Å), closer to the Al_{oct}-O distance in perfect YAG (1.95 Å) and pushing the other two oxygens (O_{b1} and O_{d1}) away to nonbonding distances (2.89 and 3.22 Å), something that can be realized because of the presence of Y_{Al} (note that single Al_Y defects maintain coordination 8, Table I). At the same time, Y_{Al} forces the six surrounding oxygens to move outward (2.13–2.23 Å) to distances closer to the original dodecahedral environment in perfect YAG (2.33 and 2.45 Å) but it is not capable of achieving its natural eightfold coordination in YAG. In order to illustrate this, the distances between Y_{Al} and its closest oxygens, O_{d3} and O_{d1}, are shown (3.78 and 4.20 Å), which are very similar to the initial Al_{oct}-O_{d3} and Al_{oct}-O_{d1} distances (3.78 and 4.31 Å). Together with these deformations around Al_Y and Y_{Al}, the Y-Al distance is significantly increased (from 3.38 to 3.66 Å), as a consequence of a softer shielding of the oxygens on the repulsion between these cations after the rearrangement of the twelve oxygens. In the same line, the AlO_4 moieties seem to be flexible enough so as to accommodate the stress produced by the oxygen rearrangement. In fact, the contraction around Al_Y is followed by a shortening of the distance between this site and Al_{tet1}, of the adjacent AlO_4 moiety that shares two oxygens with the dodecahedron (from 3.03 to 3.00 Å). This moiety responds with an enlargement of the Al_{tet1}-O distances (from 1.79 to 1.80–1.83 Å). In parallel to this, the expansion around Y_{Al} is followed by an enlargement of the distance between this site and Al_{tet2}, of the adjacent AlO_4 moiety which shares two oxygens with the octahedron (from 3.39 to 3.44 Å). This moiety responds with a shortening of the Al_{tet1}-O distances (from 1.79 to 1.75–1.78 Å), all of it resulting in a minimization of the displacements of the oxygens in the third coordination shell of the Y_{Al}-Al_Y antisite defect and a negligible distortion beyond that shell.

2. Electronic structure

The band structure of 1AD:YAG does not show important changes with respect to perfect YAG.[13,18] The total density of states (DOS) of the most stable 1AD:YAG and YAG are shown together in Fig. 5(a), where the zero reference corresponds to YAG's top of the valence band. No significant differences between 1AD:YAG and YAG are observed in Fig. 5(a); the main characters of the peaks are Y 4*p* at −20 eV, O 2*s* at −16 eV, O 2*p* between −6 and 0 eV, and Y 5*s* and 5*d* at the bottom of the conduction band. However, a closer look at the highest valence and lowest conduction states [Fig. 5(b)] reveals interesting features: some of the valence states split up by the AD formation, introducing defect levels in the gap shifted upward 0.25 eV with respect to the perfect YAG highest valence levels. An analysis of the oxygen projected DOS (PDOS) of 1AD:YAG shows that it is almost identical to the total DOS in the highest-energy region of the valence as it was the case in YAG,[18] which indicates that the gap reduction is due to changes in the electronic structure of the oxygen atoms. A Mulliken population analysis[30] of the 12 oxygens directly involved in the AD formation does not show any significant differences in the change of their total and overlap populations; however, the PDOS of the individual oxygens are revealing. They are shown in Fig. 5(c) together with the PDOS of oxygen in perfect YAG. It can be observed that the states on the three oxygens which remain at a long distance from Al_Y (O_{d2}, O_{b1}, and O_{d1}) increase their energy, the longer the distance the larger the energy increase, with a very significant change in the two oxygens at 2.9 Å(O_{b1}) and 3.2 Å(O_{d1}); these are very long compared with usual Al-O distances and the two oxygens might be considered basically unbound to Al_Y. O_{b1} and O_{d1} present a very similar PDOS profile, though shifted with respect to each other. Of these two oxygens, O_{b1} was initially a bridge atom sharing the coordinations of the ref-

TABLE II. Calculated defect formation energies, E_f, and relaxation energies, E_r, in eV per antisite defect. In parentheses, differences with respect to structure A1. Calculated binding energies, E_b, between Y_{Al} and Al_Y in 1AD:YAG and between single ADs in 2AD:YAG, in eV. 1 eV/defect=96.4853 kJ/mol.

		1AD:YAG			
Structure	$d(Y_{Al}\text{-}Al_Y)$/Å				
Figure 3	YAG	1AD	E_f(1AD) [a]	E_r(1AD) [b]	E_b(1AD) [c]
1	3.39	3.65	3.72 (0.11)	−6.18 (0.14)	0.74
2	5.46	5.33	4.02 (0.41)	−5.86 (0.46)	0.44
3	6.94	6.50	4.08 (0.47)	−5.81 (0.51)	0.36
4	8.16	8.16	4.32 (0.71)	−5.56 (0.76)	0.14
	∞	∞	4.46 (0.85)	−5.44 (0.88)	

	2AD:YAG		
Structure	E_f(2AD) [d]	E_r(2AD) [e]	E_b(2AD) [f]
Alternated series (Fig. 6)			
A1	3.61 (0.00)	−6.32 (0.00)	0.22
A2	3.68 (0.07)	−6.22 (0.10)	0.08
A3	3.70 (0.09)	−6.19 (0.13)	0.04
A4	3.74 (0.13)	−6.15 (0.17)	−0.04
Contiguous series (Fig. 7)			
C1	3.83 (0.22)	−6.10 (0.22)	−0.22
C2	3.84 (0.23)	−6.08 (0.24)	−0.24
C3	3.89 (0.28)	−6.05 (0.27)	−0.34
C4	3.91 (0.30)	−6.03 (0.29)	−0.38
C5	3.93 (0.32)	−6.01 (0.31)	−0.42
C6	3.94 (0.33)	−6.00 (0.32)	−0.44

[a] $E_f(1AD)=E(1AD)-E(YAG)$.
[b] $E_r(1AD)=E(1AD)-E_0(1AD)$.
[c] $E_b(1AD)=E_{f,\infty}(1AD)-E_f(1AD)$.
[d] $E_f(2AD)=[(E2AD)-E(YAG)/2]$.
[e] $E_r(2AD)=[E(2AD)-E_0(2AD)]/2$.
[f] $E_b(2AD)=2E_f[1AD(\text{structure } 1)]-2E_f(2AD)$.

erence Y and Al atoms in YAG and it becomes unbound to Al_Y and remains bound only to Y_{Al} in 1AD:YAG (besides to the other two on-site atoms Y and Al_{tet}; note that each O atom in YAG is bound to one Al_{oct}, one Al_{tet}, and two Y atoms). O_{d1}, however, which was not bound to the reference Al_{oct} atom in YAG and was only bound to the reference Y, is now basically unbound to Al_Y in 1AD:YAG. It is around this oxygen where the highest valence states 0.25 eV above those of YAG are localized.

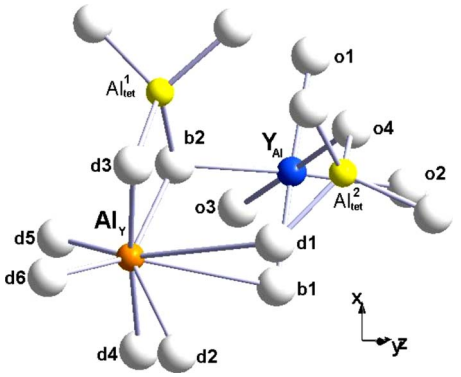

FIG. 4. (Color online) Relaxed structure of the most stable 1AD:YAG [Fig. 3 (1)]. Al_Y [orange (medium-light gray)], Y_{Al} [blue (medium-dark gray)], and adjacent Al_{tet} atoms [yellow (light gray)] shown. Oxygen labels according to Fig. 2.

B. Two antisite defects per unit cell, 2AD:YAG

1. Structure

The study of two antisite defects per unit cell, 2AD:YAG, is largely simplified by considering only AD pairs made of the most stable single ADs, where Y_{Al} and Al_Y lie at the closest distance (Sec. III A). This, together with the fact that the crystal belongs to the trigonal $R\bar{3}$ space group,[4] reduces the number of 2AD:YAG cases to ten. This is so because the [111] axis, which is a $\bar{3}$ symmetry axis, contains no Y (c) sites and four Al_{oct} (a) sites, which forces the two Y_{Al} to be located along the [111] axis and the two corresponding Al_Y to distribute randomly around it. The ten cases may be

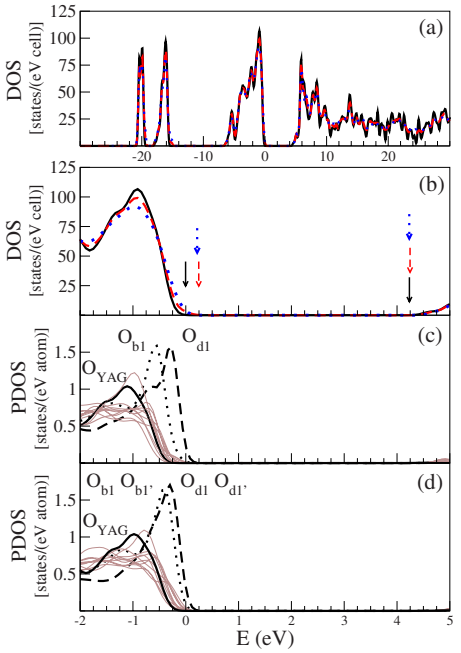

FIG. 5. (Color online) (a) Total DOS of YAG (black solid line), 1AD:YAG (red dashed line), and 2AD:YAG (blue dotted line). (b) Zoom over the gap zone. Vertical arrows indicate the end of the valence bands and the beginning of the conduction bands [same lines as in (a)]. (c) PDOS for the 1AD:YAG oxygen atoms shown in Fig. 4. (d) PDOS for the 2AD:YAG oxygen atoms shown in Fig. 8. In (c) and (d), dashed and dotted lines are used for the distinctive oxygens with indicated labels; thin lines are used for the remaining oxygens of the respective figures. The oxygen PDOS of perfect YAG is shown as a reference.

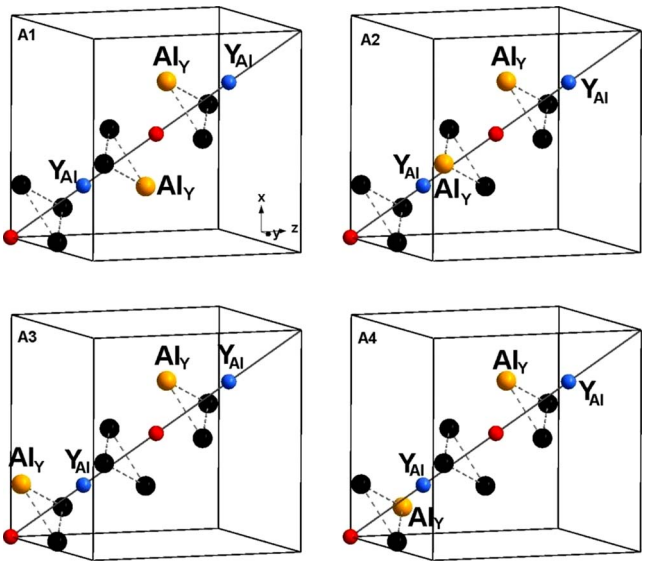

FIG. 6. (Color online) Studied double 1AD:YAG with alternated Y_{Al} positions. [111] axis shown. Positions before structural relaxation. Colors: Al_Y atoms, orange (medium-light gray); Y_{Al} atoms, blue (medium-dark gray); Y atoms, black; and Al_{oct} atoms, red (dark gray).

grouped in a series of four cases where the two Y_{Al} substitutions are *alternated* (Fig. 6) and another series of six cases where they are *contiguous* (Fig. 7).

The formation energies per AD of all the ten cases, E_f(2AD), calculated out of the total energies per unit cell of the relaxed structures as $[E(2AD)-E(YAG)/2]$, corresponding relaxation energies per AD, E_r(2AD), and binding energies between the two single ADs, E_b(2AD), in each studied 2AD:YAG case are shown in Table II. According to these calculations, two independent single ADs attract each other so that the most stable 2AD:YAG is energetically more favorable than two separated single ADs with a binding energy of 0.22 eV (0.11 eV/AD and 10.7 kJ/mol). This situation presents as well the most favorable relaxation energy per AD. From binding energies in Table II, it can be observed that not all the 2AD configurations are binding. The alternated distribution of the ADs, with the atomic sequence $\cdots$-Al_{oct}-Y_{Al}-Al_{oct}-Y_{Al}-$\cdots$ all along the [111] axis, is more stable than the contiguous distribution, with the atomic sequence $\cdots$-Al_{oct}-Al_{oct}-Y_{Al}-Y_{Al}-$\cdots$. Forming pairs of adjacent ADs has an energy cost of 0.2–0.3 eV/defect (20–30 kJ/mol) over distributing them evenly along the [111] axis. On the other hand, the energies of all the alternated structures are not very different. The two alternated structures whose Y_{Al}-Al_Y vectors have an antiparallel projection on the [111] axis (A1 and A2), and somehow tend to oppose each other and diminish the local dipole moment, are more stable than the other two alternated structures (A3 and A4), whose Y_{Al}-Al_Y vectors have a parallel projection on the [111] axis and tend to back each other and increase the local dipole moment. Among all, the most stable structure is A1, which is shown in Fig. 8 and is the only one with inversion symmetry respect to the unit-cell center. Because of this, it is the only structure of 2AD:YAG with zero local dipole moment with respect to (1/2,1/2,1/2). Some of its structural details are presented in Table III. The local structures of the two antisite defects are identical as a consequence of the inversion center at the Al_{oct} (1/2,1/2,1/2) site and they are very similar to the structure of a single AD. In particular, they show the interesting features of one bridge oxygen between Al and Y becoming only bound to Y_{Al} (O_{b1} and $O_{b1'}$) and one oxygen initially bound to Y becoming unbound to Al_Y (O_{d1} and $O_{d1'}$). In this structure, the Al_{oct} atom linking the two ADs seems to play an important role in its stability because the Al_{oct}-O distances shorten from the initial value in YAG, 1.95 Å, to 1.89, 1.91, and 1.94 Å, closer to Al-O distances in other compounds, such as 1.86 Å in Al_2O_3 (Ref. 31) and 1.89 Å in $LaAlO_3$.[32]

2. Electronic structure

The total DOS of the most stable 2AD:YAG structure (A1) is shown in Figs. 5(a) and 5(b). The same features observed in 1AD:YAG are reproduced in 2AD:YAG, presenting defect levels in the gap, which results from an energy shift of approximately 0.21 eV of the two oxygen atoms O_{b1} and O_{d1} (and their symmetry equivalents $O_{b1'}$ and $O_{d1'}$), which correspond to oxygens O_{b1} and O_{d1} in 1AD:YAG and are unbound to Al_Y, as it is demonstrated in the PDOS in Fig. 5(d). In other words, the most stable 2AD:YAG structure shows basically the same electronic structure as

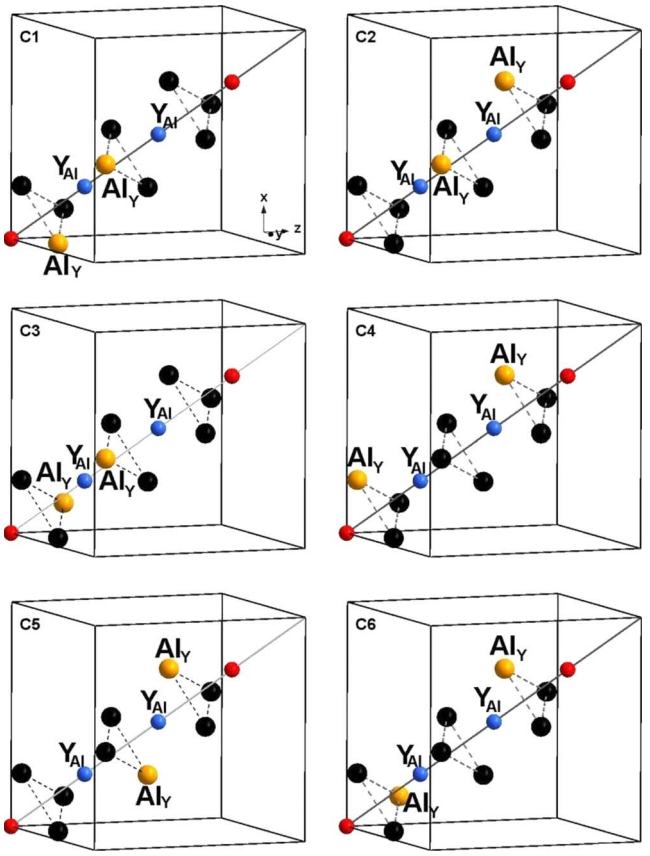

FIG. 7. (Color online) Studied double 1AD:YAG with contiguous Y_{Al} positions. [111] axis shown. Positions before structural relaxation. Colors: Al_Y atoms, orange (medium-light gray); Y_{Al} atoms, blue (medium-dark gray); Y atoms, black; and Al_{oct} atoms, red (dark gray).

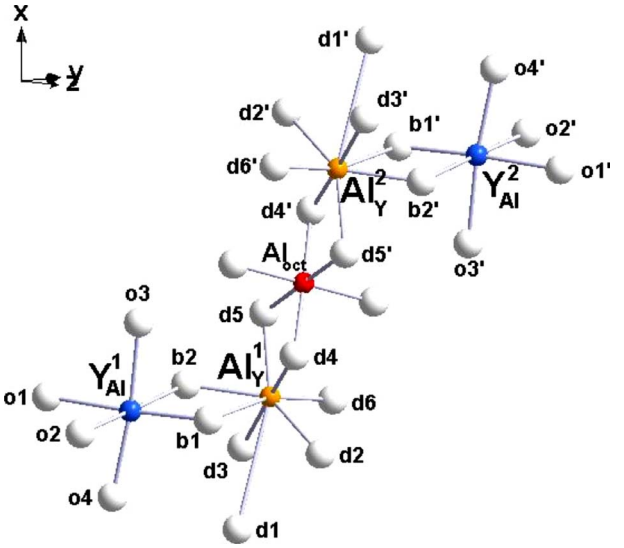

FIG. 8. (Color online) Relaxed structure of the most stable 2AD:YAG [Fig. 6 (A1)]. Al_Y [orange (medium-light gray)], Y_{Al} [blue (medium-dark gray)], and linking Al_{oct} atom [red (dark gray)] shown. Oxygen labels according to Fig. 2.

TABLE III. Al-O and Y-O distances of the most stable 2AD:YAG structure (Fig. 8), in Å.

Dodecahedral sites		Octahedral sites	
Oxygen	$d(Al_Y\text{-O})$	Oxygen	$d(Y_{Al}\text{-O})$
d1	3.34	o1	2.22
b1	2.86	o2	2.22
d2	2.10	o3	2.22
d3	2.17	b2	2.21
b2	2.06	o4	2.19
d4	2.06	b1	2.12
d5	2.08	d3[a]	4.19
d6	1.97	d1[a]	3.86

[a]This oxygen does not belong to the first, sixfold coordination shell of Al_{oct} in YAG.

1AD:YAG as a consequence of it being made of two almost independent single antisite defects linked by a AlO_6 moiety.

IV. CONCLUSIONS

First-principles DFT-GGA calculations with the PBE functional have been made on the atomistic structure, electronic structure, and distribution of antisite defects in YAG in concentrations of one and two ADs per unit cell. The interactions between the two substitutional defects that make up an AD, Y_{Al} and Al_Y, could in principle be assigned to both electrostatics and mediated by strain. All observations fit in very naturally with induced multipole interactions, although we are aware we have not ruled out other pictures. The most stable single AD is made of the Y_{Al} and Al_Y as close as possible, presenting a binding energy of 0.74 eV with respect to the individual substitutional defects. While Y_{Al} maintains the original sixfold coordination of AlO_6 and increases all Y_{Al}-O distances, Al_Y cannot retain two of the eight oxygen atoms of the original YO_8 dodecahedral moiety, which move away, and lowers significantly six of the Al_Y-O distances, becoming sixfold coordinated. One of the two oxygen atoms which become unbound to Al_Y is one of the two bridge oxygens between YO_8 and AlO_6 in perfect YAG; the other belongs only to YO_8 in YAG. As a consequence of their being less tightly bound to a cation, the upper electronic levels localized in these oxygens shift upward, especially those on the latter, introducing levels in the gap of perfect YAG 0.25 eV above the top of the valence band. The formations of one and two antisite defects per unit cell are endothermic and the formation energy per defect is lower in 2AD than in 1AD. The most stable 2AD:YAG structure is the only one which preserves the inversion center with respect to (1/2,1/2,1/2) and, in consequence, has zero dipole moment with respect to the unit-cell center. It is made of two single ADs linked by a AlO_8 moiety, which seems to play an important role in the stability of the structure. It has basically the same electronic structure as the most stable single AD and presents a binding energy between the two ADs of 0.22 eV.

ACKNOWLEDGMENTS

This work was partly supported by a grant from Ministerio de Ciencia e Innovación, Spain (Dirección General de Programas y Transferencia de Conocimiento under Grant No. MAT2008-05379/MAT). These calculations have been performed using the CamGRID computational structure. A.B.M.-G. acknowledges the hospitality and helpfulness of people of the Department of Earth Sciences (University of Cambridge, U.K.) and a contract of the program Personal Investigador en Formación (Comunidad de Madrid).

[1] G. deWith, in *High Technology Ceramics*, edited by P. Vincenzini (Elsevier, Amsterdam, 1987), p. 2063.
[2] R. C. Powell, *Physics of Solid State Laser Materials* (AIP, New York, 1998).
[3] T. Justel, H. Nikol, and C. Ronda, Angew. Chem., Int. Ed. **37**, 3084 (1998).
[4] J. Dong and K. Lu, Phys. Rev. B **43**, 8808 (1991).
[5] F. A. Selim, D. Solodovnikov, M. H. Weber, and K. G. Lynn, Appl. Phys. Lett. **91**, 104105 (2007).
[6] V. Babin, K. Blazek, A. Krasnikov, K. Nejezchleb, M. Nikl, T. Savikhina, and S. Zazubovich, Phys. Status Solidi C **2**, 97 (2005).
[7] Y. Zorenko, A. Voloshinovskii, I. Konstankevych, V. Kolobanov, V. Mikhailin, and D. Spassky, Radiat. Meas. **38**, 677 (2004).
[8] Yu. Zorenko, A. Voloshinovskii, V. Savchyn, T. Voznyak, M. Nikl, K. Nejezchleb, V. Mikhailin, V. Kolobanov, and D. Spassky, Phys. Status Solidi B **244**, 2180 (2007).
[9] F. Euler and J. A. Bruce, Acta Crystallogr. **19**, 971 (1965).
[10] C. Landron, S. Lefloch, M. Gervais, J. P. Coutures, and D. Bazin, Phys. Status Solidi B **196**, 25 (1996).
[11] M. Kuklja, J. Phys.: Condens. Matter **12**, 2953 (2000).
[12] C. Milanese, V. Buscaglia, F. Maglia, and U. Anselmi-Tamburini, Chem. Mater. **16**, 1232 (2004).
[13] Y.-N. Xu and W. Y. Ching, Phys. Rev. B **59**, 10530 (1999).
[14] G. Pari, A. Mookerjee, and A. K. Bhattacharya, Physica B **365**, 163 (2005).
[15] F. Pascale, C. M. Zicovich-Wilson, R. Orlando, C. Roetti, P. Ugliengo, and R. Dovesi, J. Phys. Chem. B **109**, 6146 (2005).
[16] M. G. Shelyapina, V. S. Kasperovich, and P. Wolfers, J. Phys. Chem. Solids **67**, 720 (2006).
[17] C. L. Freeman, N. L. Allan, and W. van Westrenen, Phys. Rev. B **74**, 134203 (2006).
[18] A. B. Muñoz-García, E. Anglada, and L. Seijo, Int. J. Quantum Chem. **109**, 1991 (2009).
[19] J. Gracia, L. Seijo, Z. Barandiarán, D. Curulla, H. Niemansverdriet, and W. van Gennip, J. Lumin. **128**, 1248 (2008).
[20] P. Hohenberg and W. Kohn, Phys. Rev. **136**, B864 (1964).
[21] W. Kohn and L. J. Sham, Phys. Rev. **140**, A1133 (1965).
[22] J. M. Soler, E. Artacho, J. D. Gale, A. García, J. Junquera, P. Ordejón, and D. Sánchez-Portal, J. Phys.: Condens. Matter **14**, 2745 (2002).
[23] P. Ordejón, E. Artacho, and J. M. Soler, Phys. Rev. B **53**, R10441 (1996).
[24] J. P. Perdew, K. Burke, and M. Ernzerhof, Phys. Rev. Lett. **77**, 3865 (1996).
[25] J. Perdew, K. Burke, and M. Ernzerhof, Phys. Rev. Lett. **78**, 1396 (1997).
[26] N. Troullier and J. L. Martins, Phys. Rev. B **43**, 1993 (1991).
[27] L. Kleinman and D. M. Bylander, Phys. Rev. Lett. **48**, 1425 (1982).
[28] S. G. Louie, S. Froyen, and M. L. Cohen, Phys. Rev. B **26**, 1738 (1982).
[29] E. Anglada, J. M. Soler, J. Junquera, and E. Artacho, Phys. Rev. B **66**, 205101 (2002).
[30] R. S. Mulliken, J. Chem. Phys. **23**, 1833 (1955).
[31] I. O. T. Goto, O. L. Anderson, and S. Yamamoto, J. Geophys. Res. **94**, 7588 (1989).
[32] S. A. Hayward, F. D. Morrison, S. A. T. Redfern, E. K. H. Salje, J. F. Scott, K. S. Knight, S. Tarantino, A. M. Glazer, V. Shuvaeva, P. Daniel, M. Zhang, and M. A. Carpenter, Phys. Rev. B **72**, 054110 (2005).